Electronic Supplementary Material (ESI) for Reaction Chemistry & Engineering.
This journal is © The Royal Society of Chemistry 2020

Toluene Photocatalytic Degradation: Braiding Physico-Chemical an Intrinsic Kinetic Analyses

Uriel Caudillo-Flores,[1] *Marcos Fernández-García,* [1,*] *Anna Kubacka,*[1,*]

[1] Instituto de Catálisis y Petroleoquímica, CSIC, C/Marie Curie 2, 28049-Madrid, Spain

1. Catalytic set-up and details

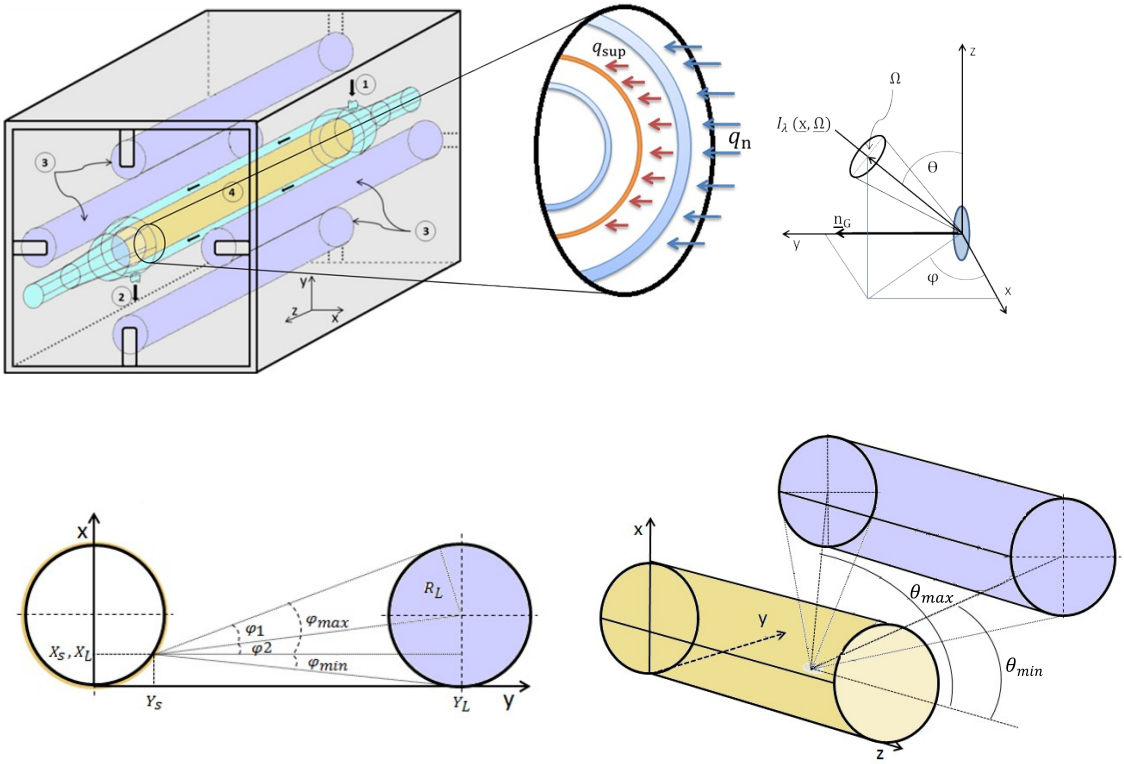

Figure S1. Upper, Left: Photocatalytic annular reactor scheme. (1) gas inlet, (2) gas outlet, (3) lamps, (4) catalyst (brown) sample. q_{sup} radiation flow on the surface of the sample (red), q_n radiation flow from the lamps (blue). Upper, Right: Center of coordinates located at the sample (defined by coordinates x_s, y_s, z_s). Down, Coordinate system to define the integration limits of radiation Model. (Left) φ_{min} and φ_{max}. (Right) Θ_{min} and Θ_{max}.

Integration limits of equation 8 are summarized in equations S1-S7 and can be graphically visualized in Figure S1.

$$\varphi_1 = \tan^{-1}\left(\frac{X_L - Xs}{Y_L - Ys}\right) \quad \text{(S1)}$$

$$\varphi_2 = \sin^{-1}\left(\frac{R_L}{\left(X_L - X_s\right)^2 + \left(Y_L - Y_s\right)^2}\right)$$

(S2)

$$\varphi_{min} = \varphi_1 - \varphi_2 \quad \text{(S3)}$$

$$\varphi_{max} = \varphi_1 + \varphi_2 \quad \text{(S4)}$$

$$\Theta_{min}(\varphi) = \cos^{-1}\frac{-Z_s}{\left(X_{Lm}(\varphi) - X_s\right)^2 + \left(Y_{Lm}(\varphi) - Y_s\right)^2 + {Z_s}^2}$$

(S5)

$$\Theta_{max}(\varphi) = \cos^{-1}\frac{Z_L - Z_s}{\left(X_{Lm}(\varphi) - X_s\right)^2 + \left(Y_{Lm}(\varphi) - Y_s\right)^2 + {Z_s}^2}$$

(S6)

Where:

$$X_{Lm}(\varphi) = X_L + \left(X_s - Y_L\right)\cos\varphi^2 + \left(Y_L - Y_s\right)(\cos\varphi \sin\varphi) - \sin\varphi\sqrt{({R_L}^2 - \left(X_s - X_L\right)}$$

(S7)

$$Y_{Lm}(\varphi) = Ys_i + \left(Y_L - Y_s\right)\cos\varphi^2 + \left(X_s - X_L\right)(\cos\varphi \sin\varphi) - \cos\varphi\sqrt{({R_L}^2 - \left(X_s - X_L\right)}$$

(S8)

Where symbols were previously defined (main text) except X_L, Y_L, Z_L which are the coordinates of the points located on the surface of the lamp.

2.- Mass balance

According to the thermo-photo reactor geometry (Fig. S1) and taking into account the following assumptions: (i) Newtonian fluid, (ii) unidirectional axial flow, (iii) azimuthal symmetry, (iv) constant physical properties, (v) negligible velocity profiles in r coordinate, (vi) negligible axial diffusion when compared to the convective flux in that direction, and (vii) negligible homogeneous photochemical reactions and (viii) steady

state condition, the a chemical reactive/product (RP) mass balance can be expressed by Eq. S9.[1]

$$v_z(r)\left(\frac{\partial C_{C_{RP}}(r,z)}{dz}\right) + \frac{D_{C_{RP}\text{ - }Air}}{r}\frac{\partial}{dr}\left(r\frac{\partial C_{C_{RP}}(r,z)}{dr}\right) = 0 \qquad \text{S9}$$

Two boundary conditions in r (Eqs. S10 and S11) and one boundary condition in z (Eq. S12) are necessary. Note that Eq. S10 includes the reaction rate for reactive consumption or product generation.

$$D_{RP\text{ - }Air}\frac{\partial C_{C_{RP}}(r,z)(r = R, z)}{dr} = \pm\, r_{C_{RP}} \qquad \text{S10}$$

$$D_{RP\text{ - }Air}\frac{\partial C_{C_3H_8O}(r,z)(r = R_e, z)}{dr} = 0 \qquad \text{S11}$$

$$C_{C_{RP}}(z = 0) = C_{C_{RP'0}} \qquad \text{S12}$$

If the reactor operates under a kinetic control regime, the mass balance can be expressed as Eq. S13:

$$v_z\left(\frac{dC_{C_{RP}}}{dz}\right) = \pm\, a\, r_{C_{RP}} \qquad \text{S13}$$

The numerical solution of Eq S13, requires one initial condition, previously defined by Eq. S12.

3.- External and internal diffusion

To determine if the external mass transfer resistance was significant, the modified Mear's criterion (C_M) was used (Eq. S14).[2]

$$\frac{\langle r\rangle_{A_c}\, n}{k_c\langle C_b\rangle_V} < 0.1 \qquad \text{S14}$$

Where:

$$\langle r \rangle_{A_c} = \frac{Q\ (C_{out} - C_{in})}{m_c\ BET}$$

S15

The influences of internal mass transfer were assessed by using the Weisz-Prater Criterion modified (Eq. S16).[3]

$$\frac{\langle r \rangle_{A_c}\ r_{eq}^2}{D_{eff} C_s} < 1$$

S16

where:

$\langle r \rangle_{A_c}$: average reaction rate (mol m^{-2} s^{-1})

n: reaction order (assumed to be 1 for acetaldehyde)

k_c: mass transfer coefficient (m s^{-1})

$\langle C_b \rangle_V$: bulk average concentration (mol m^{-3})

Q: volumetric flow rate (m^3 s^{-1})

C_{out}: outlet concentration (mol m^3)

C_{in}: inlet concentration (mol m^3)

m_c: mass (g)

BET: BET surface area (m^2 g^{-1})

r_{eq}: equivalent radius (m)

C_s: film superficial concentration (mol m^{-3})

C_M and C_{WP} values are below $1x10^{-7}$ in all cases here studied.

4. Radical formation rate measurement using EPR and optical properties

Considering that the scattering contribution can be neglected (due to the limited cross section of the cell with respect to the secondary –aggregate- particle size of the catalysts; see dimension details of the EPR cell in the Figure S2) the Local Volumetric Rate of Photon Absorption at the EPR cell can be obtained using Eq. S17 (Equations for φ and Θ integration limits are presented in Eqs. S18-S23).

$$e^{a,v}(x,y,z,C) = \sum_{L=1}^{L=2} \int_{\varphi_{min}}^{\varphi_{max}} \int_{\Theta_{min}}^{\Theta_{max}} \frac{P_{\lambda,L}}{2\pi^2 R_L Z_L} \frac{A_c}{V_c} T_{EPR-gl,\lambda}\, a_{s,\lambda}(C,y)\, sin^2\varphi\, sin\Theta\, d\varphi d\Theta \quad \text{(S17)}$$

$$\varphi_{min} = \tan^{-1}\left(\frac{X_L - X_{susp}}{Y_L - Y_{susp}}\right) - \sin^{-1}\left(\frac{R_L}{\left(X_L - X_{susp}\right)^2 + \left(Y_L - Y_{susp}\right)^2}\right) \quad \text{(S18)}$$

$$\varphi_{max} = \tan^{-1}\left(\frac{X_L - X_{susp}}{Y_L - Y_{susp}}\right) + \sin^{-1}\left(\frac{RL}{\left(X_L - X_{susp}\right)^2 + \left(Y_L - Y_{susp}\right)^2}\right) \quad \text{(S19)}$$

$$\Theta_{min}(\varphi) = \cos^{-1}\frac{-Z_{susp}}{\left(X_{Ls}(\varphi) - X_{susp}\right)^2 + \left(Y_{Ls}(\varphi) - Y_{susp}\right)^2 + Z_s^{\,2}} \quad \text{(S20)}$$

$$\Theta_{max}(\varphi) = \cos^{-1}\frac{Z_L - Z_{susp}}{\left(X_{Ls}(\varphi) - X_{susp}\right)^2 + \left(Y_{Ls}(\varphi) - Y_{susp}\right)^2 + Z_s^{\,2}} \quad \text{(S21)}$$

Where:

$$X_{Ls}(\varphi) = X_L + \left(X_{susp} - Y_L\right)\cos\varphi^2 + \left(Y_L - Y_{susp}\right)(\cos\varphi\, \text{sen}\,\varphi) - \text{sen}\,\varphi\sqrt{(R_L^{\,2} - (X_s \quad \text{(S22)}$$

$$Y_{Ls}(\varphi) = Ys_i + (Y_L - Y_{susp})\cos\varphi^2 + (X_{susp} - X_L)(\cos\varphi \operatorname{sen}\varphi) - \cos\varphi \sqrt{(R_L^2 - (X \quad \text{(S23)}$$

Where A_c, V_c and C are the superficial area of the cell (x,z-Plane), the cell volume and the suspension concentration in the cell, respectively. The optical properties of the EPR glass cell ($T_{EPR-gl,\lambda}$) and the catalyst suspension $a_{s,\lambda}(C,y)$ were determined from spectral transmittance measurements (as defined in the main text). X_L, Y_L and Z_L, are the coordinates of the points located on the surface of the lamp. X_{susp}, $Y_{susp}$and Z_{susp} are the coordinates of the points evaluated in the suspension volume.

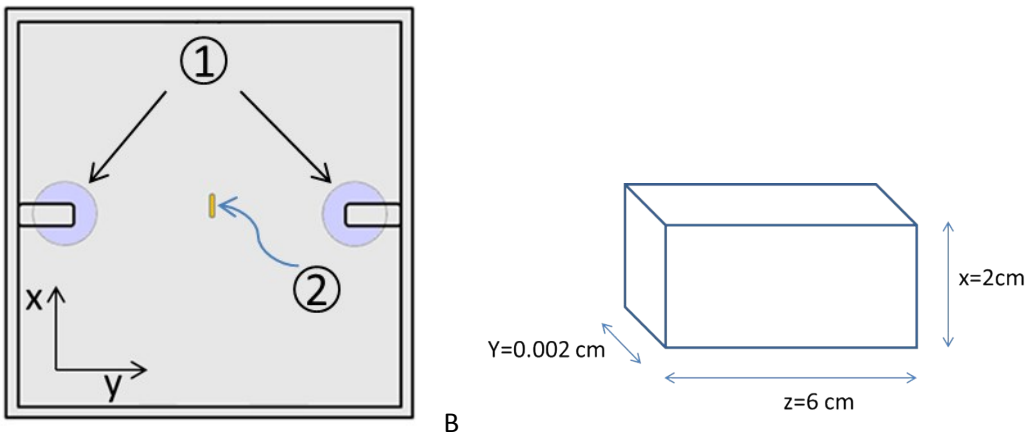

B

Figure S2. (A) Side section view of the EPR reaction system. (1) Lamps, (2). EPR cell. (B) Scheme and dimension of the EPR cell.

To obtain the kinetic expression for OH radical formation we use the kinetic formalisms summarized in Table S1. The OH measurements at the EPR cell are modelled by the initial light absorption (step 0), formation of hydroxyl radicals (step 1), concomitant formation of superoxide radical (step 2, not relevant for OH formation) and recombination of charge carriers (step 3).

Table S1. Kinetic formalism describing OH radical formation.

No.	Reaction step	Reaction rate
0	$Cat + h\nu \rightarrow Cat + h^+ + e^-$	rg
1	$h^+ + H_2O_{ads} \rightarrow OH^{\cdot} + H^+$	$k_1[H_2O]_{ads}[h^+]$
	$h^+ + OH^-_{ads} \rightarrow OH^{\bullet}$	
2	$e^- + O_{2\,ads} \rightarrow O^{\cdot-}_2$	$k_2[O_2]_{ads}[e^-]$
3	$h^+ + e^- \rightarrow heat$	$k_3[h^+][e^-]$
4	$n\,OH^{\bullet} \rightarrow Non\ radical\ species$	-

According to Table S1, more precisely, to the reaction step representing the generation of hydroxyl radicals (step 1), the rate for $OH^{\bullet}$ formation in an EPR experiment is given by:

$$r_{OH^{\bullet}} = k_1[H_2O]_{ads}[h^+] \tag{S24}$$

Where the hole concentration can be approximated considering that charge recombination in semiconductors (step 2) is expected to be much faster than any chemically related to charge decay (step 4, which does not need to be considered explicitly in Table S2). Thus, applying the steady-state approximation to the generation of holes, $k_3[h^+][e^-] = 0$, to Eq. S25:

$$\frac{r_{OH^{\bullet}}}{\sqrt{e^{a,v}}} = \sqrt{\frac{\bar{\phi}}{k_3}} k_1[H_2O]_{ads} \tag{S25}$$

Using $r_g = \bar{\phi} \sum_{\lambda} e^{a,v}_{\lambda}$

So, measuring the rate of hydroxyl formation using EPR and using the optical properties of the solids we can provide an estimation of the ratio between hole generation (k1) and recombination (k3).

5. Characterization results

Table S2. Main physico-chemical observables of the samples.

Catalyst	TiO_2 Crystallite size (nm)	WO_3 Crystallite size (nm)	BET surface area ($m^2\ g^{-1}$)	Pore volume ($cm^3\ g^{-1}$)	Pore size (nm)	Band Gap (e^-V)
Ti	11.3	-------	111.9	0.192	5.3	3.14
TiW	15.4	23.1	67.8	0.058	3.3	2.63

References

1 G. E. Imoberdorf, A. E. Cassano, H. A. Irazoqui and O. M. Alfano, *Catal. Today*, 2007, **129**, 118–126.

2 M. M. Ballari, J. Carballada, R. I. Minen, F. Salvadores, H. J. H. Brouwers, O. M. Alfano and A. E. Cassano, *Process Saf. Environ. Prot.*, 2016, **101**, 124–133.

3 G. S. Yablonsky and G. B. Marin, 2011.